Pneumatic Trail Based Slip Angle Observer with Dugoff Tire Model

Sirui Song, Michael Chi Kam Chun, Jan Huissoon, Steven L. Waslander[1]

***Abstract*— Autonomous driving requires reliable and accurate vehicle control at the limits of tire performance, which is only possible if accurate slip angle estimates are available. Recent methods have demonstrated the value of pneumatic trail for estimating slip angle in the non-linear region using the Fiala tire model. We present an improved slip angle estimation method based on the pneumatic trail method, which incorporates both lateral and longitudinal acceleration effects through the use of the Dugoff tire model. The proposed method offers significant improvements over existing methods, where longitudinal effects of the road-tire were assumed negligible. The results are demonstrated using CarSim, which relies on empirical data models for tire modelling and therefore presents a useful evaluation of the method.**

I. Introduction

Autonomous driving is gaining popularity, and promises to become the norm in the near future. Driven by the need to maximize vehicle performance, recent controller designs, such as those introduced in [5], [8], aim to operate the vehicle near the tires' friction limits. However, these controllers require precise knowledge of vehicle dynamics in order to safely operate.

Vehicle dynamics are governed by the tire-road force interaction. The maximum force generated by the tire can be illustrated through the slip circle, shown in Fig. 1. Near the centre of the slip circle, indicated by the red region, the longitudinal slip ratio and lateral slip angle are independent of each other. Near the edge of the slip circle, in the yellow region, the longitudinal and lateral slips are no longer independent, and the produced tire force is limited by maximum friction force. Outside of the slip circle, the vehicle experiences full slip, and tire performances are no longer maximized.

Given the importance of slip angle and longitudinal slip in predicting vehicle dynamics, researchers have attempted to estimate these parameters. Slip angle can be calculated using accurate GPS and Inertial Measurement Unit measurements [2]. However, due to its high sensitivity to noise, this method cannot be used with low-cost sensors available on most commercial vehicles. Motivated by this need, other estimation/observer algorithms have been proposed.

In [3] and [13], an Extended Kalman Filter (EKF) is designed to estimate the slip angles and longitudinal slips of the tires. The work presented in [3] demonstrated that the EKF performs well in the linear tire region, but is constrained in the non-linear region. Furthermore, fast convergence of the EKF is highly dependent on the accurate selection of tire parameters and vehicle models. On the other hand, a Particle Filter (PF) is able to provide more accurate estimates of slip angles, but is computationally intensive, and thus difficult to implement in real-time [13]. Another approach, using the Unscented Kalman filter (UKF), is described in [4]. While the results are promising, this estimator design is dependent on several unconventional sensors that are not commonly found on commercial vehicles.

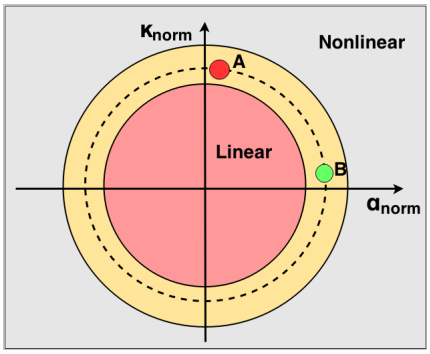

Fig. 1: Slip circle: The horizontal axis is the normalized sideslip angle, and the vertical axis is the normalized longitudinal slip ratio. Point A, high slip ratio and low slip angle, corresponds to the case when the vehicle is accelerating. Point B, low slip ratio and high slip angle, corresponds to the case when the vehicle steers aggressively. Dotted lines: vehicle driving at the limits of friction.

Recent efforts have demonstrated the benefit of using pneumatic trail to estimate tire-road behaviours, such as estimating the friction coefficient and lateral tire forces [7], [9], [14]. The pneumatic trail is a tire property encoded in the alignment moment measurements. In [7], it was found that a linear observer coupled with a pneumatic trail estimator, can accurately track the sideslip angles in both the linear and non-linear regions. Furthermore, this method is less reliant on the accuracy of model and tire parameters, uses simple calculations, and only requires sensors that are available on most commercial vehicles. However, the method presented in [7] assumes a rear wheel drive vehicle, and negligible longitudinal dynamics on the wheels. Neglecting longitudinal tire dynamics limits the accurate tracking of slip angles to areas near the horizontal axis of the slip circle. In additions, for most vehicles, especially front wheel drive vehicles, tire saturation occurs much earlier with longitudinal tire dynamics present (acceleration or braking).

In this paper, a pneumatic trail based observer design with longitudinal tire dynamics is presented. By accounting for the longitudinal dynamics, this method extends accurate slip angle estimations to the full domain of the slip circle. This observer design improves on the previous methods in two distinct areas: first, it can accurately estimate slip angle in

[1]The authors of this paper are with the faculty of Mechanical and Mechatronics Engineering at University of Waterloo in Waterloo, ON, Canada. {s7song,mchikamc,jph,stevenw}@uwaterloo.ca

both linear and non-linear regions, even with high longitudinal dynamics present; second, it can be implemented for both front wheel drive and rear wheel drive vehicles. In addition to the benefits, this observer design still uses a simple model that is not computationally intensive, and only requires input from commonly available sensors to operate.

In Section II, the fundamental elements used in the proposed algorithm are defined, including pneumatic trail, tire models and the vehicle model. The details of the observer design are presented in Section III, followed by the simulation results in Section IV. Finally, Section V presents the conclusion and future extensions.

II. Component models

A. Aligning Moment and Pneumatic Trail

The aligning moment, or self-aligning moment, is the moment that steers the tire in the direction of vehicle travel as the tire rolls [12]; it is defined by Eq. (1). The aligning moment is produced, because lateral force applies at an offset from the wheel centre, due to the elastic nature of pneumatic tires. This offset is known as pneumatic trail, t_p. For vehicles with a non-vertical steering axis due to camber angle, the aligning moment applies at an additional offset, known as the mechanical trail, t_m. Fig. 2 illustrates the relationship between lateral force, F_y, pneumatic trail, t_p, and mechanical trail, t_m for a typical pneumatic tire. In this study, the focus is on pneumatic trail, and mechanical trail is assumed constant.

$$M_z = -(t_p + t_m)F_y \tag{1}$$

where M_z is the aligning moment. Alignment moment can be measured by monitoring the torque produced by the steering assist motor, or by torque sensors mounted on the kingpins.

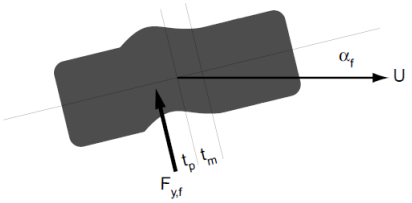

Fig. 2: In this image, U is the vehicle velocity, and $alpha_f$ is the tire slip angle. Aligning moment is produced because F_y does not apply directly at the tire's centre. As tire saturates, t_p approaches the centre, and aligning moment approaches zero. t_m is measured from the centre of the tire. [6]

B. Lateral Force and Pneumatic Trail

As the tire saturates, pneumatic trail approaches zero, and aligning moment approaches zero [9]. Eq. (2) shows a simplified pneumatic trail calculation, derived from the equation presented in [9]. It is important to note that this model is not accurate for very small small slip angles, or slip angles outside of the slip circle region. However, this equation does account for longitudinal dynamics for slip angles within the slip circle.

$$t_p = \begin{cases} t_{p0} - \dfrac{t_{p0}}{3} I_f |\sqrt{(C_1)^2 + (C_2)^2}|, & \text{if } \sigma \geq 1 \\ 0, & \text{if } \sigma < 1 \end{cases} \tag{2}$$

with

$$C_1 = \frac{C_\alpha \tan(\alpha)}{1+\kappa}, C_2 = \frac{C_\kappa \kappa}{1+\kappa} \tag{3}$$

In Eq. (2), C_α is the tire's lateral stiffness and C_κ is the longitudinal stiffness. I_f is a function of tire normal force and friction coefficient, as defined in Eq. (7). σ comes from the Dugoff tire model defined in Eq. (5). This pneumatic trail model begins at an initial trail t_{p0} and decays to zero as the limits of tire adhesion are reached. A reasonable estimate for t_{p0} is assumed to be $\frac{l}{6}$, where l is the length of the tire contact patch [9]. This model ignores the longitudinal effects due to scrub radius, which may contribute up to 4% error [10]. Some assumptions are necessary for the formulation of this equation: [9]

- There are no carcass deformations in the tires
- The tires are isotropic. This implies that unit lateral deformation is equal to the unit longitudinal deformation.
- The tire is operating at steady state, the relaxation length effects and other dynamic effects are not modelled.

C. Dugoff Tire Model

The Dugoff tire model [11] is a simple analytical model that incorporates both longitudinal and lateral dynamics to calculate the tire-road force characteristics. It assumes a steady state tire behaviour. Compared to other well known models, such as the Fiala tire model or the linear tire model [9], the Dugoff tire model is more accurate by accounting for the longitudinal tire dynamics as well as the lateral dynamics. In comparison to the more sophisticated models, such as the Pacejeka Magic Formula [9], the Dugoff tire model uses fewer parameters, and is less reliant on accurate tire parametrization. The Dugoff tire model is summarized for the front tires in Eq. (4)-(6),

$$\begin{aligned} F_{xf} &= \begin{cases} -C_\kappa \dfrac{K_f \kappa_f}{1+\kappa_f}, & a_x > 0 \\ -C_\kappa K_f \kappa_f, & a_x \leq 0 \end{cases} \\ F_{yf} &= \begin{cases} -C_\alpha \dfrac{K_f \tan(\alpha_f)}{1+\kappa_f}, & a_x > 0 \\ -C_\alpha K_f \tan(\alpha_f), & a_x \leq 0 \end{cases} \end{aligned} \tag{4}$$

with

$$K_f = \begin{cases} (2-\sigma_f)\sigma_f & \sigma_f < 1. \\ 1, & \sigma_f \geq 1. \end{cases} \tag{5}$$

$$\sigma_f = \frac{(1+\kappa_f)\mu F_{zf}}{2 I_f \sqrt{C_\kappa^2 \kappa_f^2 + C_\alpha^2 \tan^2(\alpha_f)}} \tag{6}$$

Eq. (4) presents the calculations for the longitudinal and lateral forces for a given slip angle and slip ratio, for both accelerating $a_x > 0$ and braking $a_x < 0$ conditions. κ_f and α_f are the longitudinal slip ratio and slip angle values. F_{zf} is the normal force applied on the front tire, and μ is the coefficient of friction between the tire and the ground. In this case, only the front tires formulation is presented; however, similar equations apply for the rear tires [9].

As described in [6], an observation can be made that the μ term and F_z term always appear together, in both the

Dugoff tire model and the pneumatic trail calculations. The two terms can be combined together into an inverse peak force coefficient, I_f.

$$\begin{aligned} I_f &= \frac{1}{\mu F_{zf}} \\ I_r &= \frac{I_f * F_{zf}}{F_{zr}} \end{aligned} \tag{7}$$

D. Vehicle Model

The vehicle model used in this paper is a Single Track Bicycle Model described in [9] for its simple formulation. This model does not account for vehicle dynamics such as lateral and longitudinal weight transfer. A Four Wheel Vehicle Model, as described in [13], can be used to include more details.

The vehicle model makes the following assumptions:

- Planar dynamics only, no longitudinal weight transfer
- Four wheel dynamics are combined into two wheels.
- No vertical or lateral dynamics present.

$$\begin{aligned} \dot{\beta} &= \frac{1}{mV_x}(F_{yf} + F_{yr}) - r \\ \dot{r} &= \frac{1}{I_z}(aF_{xf} - bF_{yf}) \end{aligned} \tag{8}$$

The vehicle slip angle, β, is the difference between vehicle heading and direction travelled. The vehicle yaw rate is r, and V_x is the longitudinal vehicle velocity. The length, a, is the distance between the front axle and the centre of gravity, and the length b is the distance between the rear axle and the centre of gravity. Finally, F_x and F_y are the respective longitudinal and lateral forces produced by the tires.

Assuming the vehicle is a rigid body, the relationship between the vehicle slip angle and the front and rear tire slip angles can be expressed as

$$\begin{aligned} \alpha_f &= \beta + \frac{ar}{V_x} - \delta \\ \alpha_r &= \beta - \frac{br}{V_x} \\ \alpha_r &= \alpha_f + \delta - \frac{(a+b)r}{V_x} \end{aligned} \tag{9}$$

where δ is the steering angle.

The longitudinal slip ratio is given by Eq. (10) and is the difference between the velocity of the wheel and the velocity of the vehicle,

$$\kappa = \frac{V_{xt} - V_x}{\max(V_{xt}, V_x, \epsilon)} \tag{10}$$

where V_{xt} is the velocity of the wheel, calculated as the product of the effective tire radius and the wheel rotational speed; V_x is the longitudinal velocity of the vehicle; and ϵ is a constant parameter with a small value so the denominator is not zero.

For a front wheel drive vehicle, the rear wheel does not apply driving force, longitudinal effects for the rear tires are generated by friction. For most cases, this is negligible compared to the front driving tires. We make the assumption that the longitudinal slip ratio on the rear tire is zero, or the rear tires do not slip. Therefore, the front tires slip ratio becomes Eq. (11). This calculation assumes accurate knowledge of velocity, and is only valid when the rear wheels experience negligible longitudinal slip. In cases where this does not hold true, alternative methods to estimate the slip ratio, κ, such as an EKF [3], can be used.

$$\kappa_f = \frac{V_{xf} - V_{xr}}{\max(V_{xr}, V_{xf}, \epsilon)} \tag{11}$$

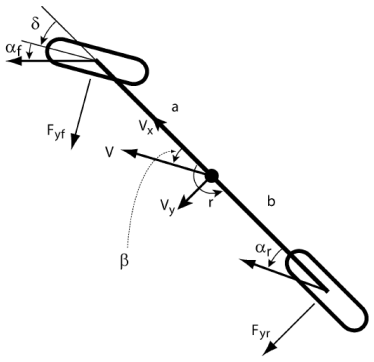

Fig. 3: Single track bicycle model [6]

III. Observer Description

The observer algorithm is described in detail below. This observer uses a linear observer with the Dugoff tire model to update the slip angles and vehicle dynamics. It also integrates a pneumatic trail estimation block to update the inverse peak force coefficient, which is used in the linear observer. Since the inverse peak force coefficient is a function of both the friction coefficient and the normal force, this set-up allows precise estimation of slip angle without having accurate knowledge of the normal force or the friction coefficient. Initially, select the nominal μ_0, F_{fz0} values, and calculate

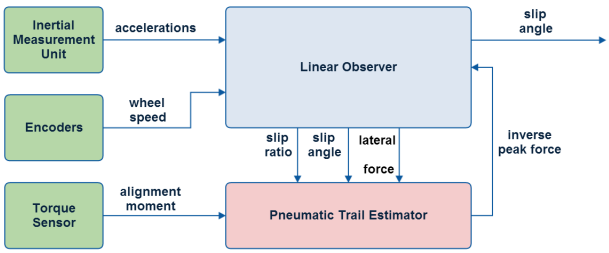

Fig. 4: Observer block structure.

an initial inverse peak force coefficient, I_f. Assuming that the vehicle starts from standstill, the estimated slip angle, $\hat{\alpha_f}$, can be set to zero. The algorithm then proceeds as follows:

1) Determine I_r from Eq. (7) and the initialized inverse peak force coefficient, I_f.
2) Using the front and rear wheel encoder data, calculate the longitudinal slip ratio estimate, $\hat{\kappa}_f$ from Eq. (11).
3) With known I_f, $\hat{\kappa}_f$, and $\hat{\alpha}_f$, lateral force, $\hat{F}_{yf}$ can be calculated using the Dugoff tire model presented in Eq. (4).
4) Calculate $\dot{\alpha}_f$ from Eq. (9) and the Single Track Bicycle Model (Eq. (8)). Note that this derivation does not

assume a constant V_x, and accounts for the longitudinal dynamics of the vehicle.

$$\dot{\alpha}_f = (\frac{1}{mV_x} + \frac{a^2}{I_z V_x})F_{yf} + (\frac{1}{mV_x} - \frac{ab}{I_z V_x})F_{yr} - r - \frac{ar\dot{V}_y}{(V_x^2)} - \dot{\delta}. \tag{12}$$

The observer update rule is described as,

$$\dot{\hat{\alpha}}_f = (\frac{1}{mV_x} + \frac{a^2}{I_z V_x})\hat{F}_{yf} + (\frac{1}{mV_x} - \frac{ab}{I_z V_x})\hat{F}_{yr} - r - \frac{ar\dot{V}_y}{(V_x^2)} - \dot{\delta} + K(\hat{F}_{yf} - \tilde{F}_{yf}). \tag{13}$$

where K is the observer gain, and $\tilde{F}_{yf}$ is given by:

$$\tilde{F}_{yf} = ma_y - \hat{F}_{yr} \tag{14}$$

5) Calculate $\hat{\alpha}_f$ by integrating the observer update rule.
6) Determine $\hat{\alpha}_r$ from $\hat{\alpha}_f$ using Eq. (9)
7) With the estimated $\hat{F}_{yf}$, update $\hat{t}_p$ based on the measured aligning moment, using Eq. (1).
8) Update I_f by rearranging Eq. (2) and substituting in $\hat{t}_p$ and $\hat{\alpha}_f$.

$$I_f = \begin{cases} \dfrac{3(t_{p0} - \hat{t}_p)}{\left|\sqrt{(\hat{C}_1)^2 + (\hat{C}_2)^2}\right|}, & \sigma_f \geq 1 \\ \dfrac{1}{\mu_0 F_{z0}}, & \sigma_f < 1 \end{cases} \tag{15}$$

with

$$\hat{C}_1 = \frac{C_{\kappa_f}\hat{\kappa}_f}{1+\hat{\kappa}_f}, \hat{C}_2 = \frac{C_{\alpha_f}\tan(\hat{\alpha}_f)}{1+\hat{\kappa}_f} \tag{16}$$

9) Substitute the updated inverse peak force coefficient, I_f, into step 1, and repeat the process.

IV. Simulation

A. Simulation Set-up

The observer is verified using a high fidelity vehicle model in CarSim, which is based on tire models discussed in [1] and [9]. The vehicle model captures the vehicle dynamics such as longitudinal and lateral dynamics, aerodynamics effects, steering and wheel geometry etc.. The tire model used is derived from empirical test data. The vehicle simulated is a mid-size sedan with $m = 1650kg$, $a = 1.4m$, $b = 1.65m$, $Iz = 3234kgm^2$. The tire parameters are defined as $C_\alpha = 89000N/rad$, $C_\kappa = 75000N$. The road surface has a constant $\mu = 0.7$.

Random Gaussian noise is added to each sensor measurement. The sensors and the estimation loop both update at 100 Hz with the following noises variances: encoder: $1.2m/s$; IMU linear acceleration: $2.25m/s^2$; IMU yaw rate: $2degree/s$; torque sensor: $2.25Nm$.

Three estimation techniques are compared in the following simulation:

LL: Linear observer with longitudinal dynamics.

LP: Linear observer with lateral dynamics and pneumatic trail estimation, as implemented in [6].

LLP: Linear observer with longitudinal dynamics and pneumatic trail estimation method presented in this paper.

The performances of the three estimation techniques are compared in the following test scenarios: constant steering with delayed constant longitudinal acceleration, slalom steering with delayed constant longitudinal acceleration, and ramp steering with delayed constant longitudinal acceleration.

The constant steering test is used as a baseline to compare the observers' performances in both driving scenarios with little longitudinal dynamics, and that with high longitudinal dynamics present. In this test, the vehicle steering angle is maintained at a constant 3 degrees. From 0s to 40s, the vehicle accelerates to 20km/h and maintains this speed. From 40s to 110s, the vehicle accelerates at a maximum of 10km/h/s.

The slalom test is useful in judging observers' performances in extreme driving scenarios. In this test, the vehicle steering angle oscillates in a sine wave with an amplitude of 5 degrees and frequency of 0.35 rad. Similar to the constant steering test, the vehicle initially accelerates to 20km/h and maintains this speed for 40 seconds; it then accelerates longitudinally at a maximum of 5km/h/s for 50s.

The ramp steering test is used to compare the performances of the three observers in scenarios with prolonged operations at the limit of tire stability. For the first 15 seconds of the test, the vehicle maintains a 4.5 degrees steering angle. For the next 35 seconds, the vehicle increases its steering angle at 0.5 degrees/s until its maximum steering angle. The longitudinal input is identical to that in the slalom test.

B. Results and Discussions

In the constant steering test, shown by Fig. 5, two observations can be made. Firstly, the velocity measurement is realistic in simulating the sensor noise. Furthermore, the small periodic spikes in the longitudinal slip ratio are due to gear changes.

In Fig. 8, from t = 0s to 40s, the longitudinal dynamics are not significant; $\kappa \approx 0$. During this period, all three estimation methods track slip angles well; however, LL appears to be more noisy than the other observers. Pneumatic trail blocks in LP and LLP eliminate some noises.

From t = 50s to 110s, the effects of longitudinal dynamics become noticeable; $\kappa \approx 0.05$. LP estimates begin to deviate from the actual slip angle measurements. This is because LP does not model longitudinal slip.

From t = 110s to 150s, the front tires are fully saturated, and longitudinal slip become significant as $\kappa \approx 0.1$. LP significantly underestimates the slip angle, but both LL and LLP track the slip angle well into the non-linear region ($\alpha \geq 10$ degrees) with an average errors less than ± 3 degrees.

In the slalom steering test shown by Fig. 6 and Fig. 9, similar observations to the constant steering test can be made, with the following additions: From t = 0s to 5s, LL produces a noticeable amount of noise and bias in the linear region,

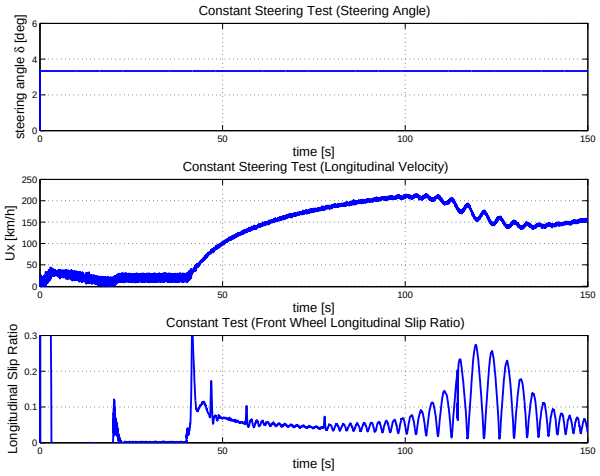

Fig. 5: Constant steering manoeuvre

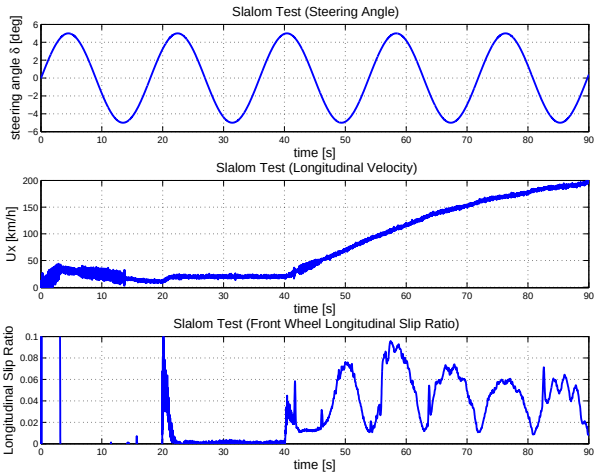

Fig. 6: Slalom test manoeuvre

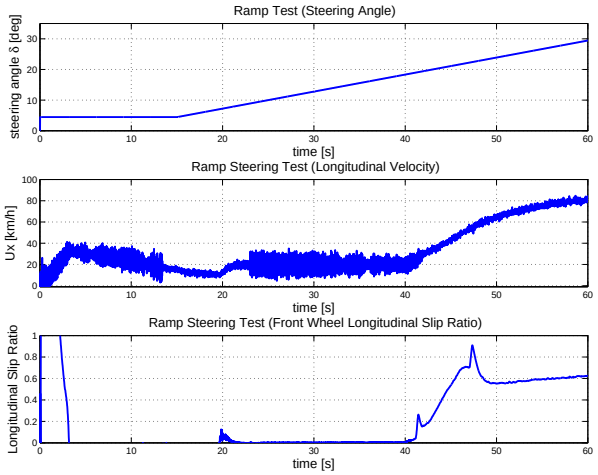

Fig. 7: Ramp test manoeuvre

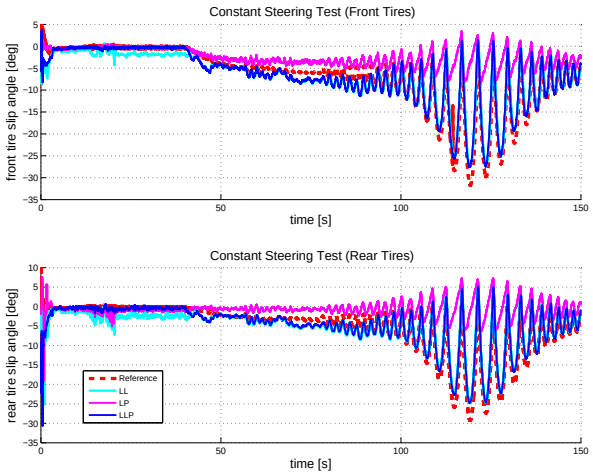

Fig. 8: Constant steering test results

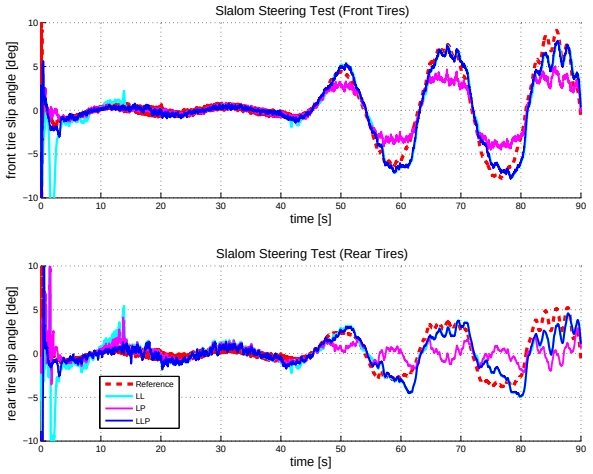

Fig. 9: Slalom simulation results

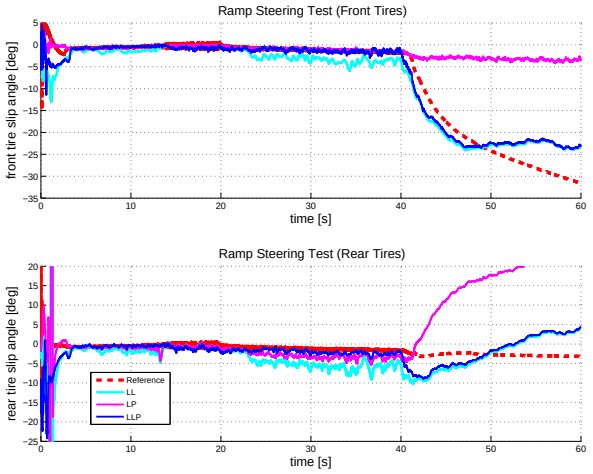

Fig. 10: Ramp test simulation results

especially when the vehicle is shifting gear. Nonetheless, LLP is able to adapt to the gear change, and track the actual slip angle with an average error smaller than 1 degree. From t = 40s to 90s, LLP is able to track the slip angle in the non-linear region, whereas LP plateaus when high longitudinal slip is present.

In the ramp steering test, Fig. 7 and Fig. 10, similar observations can be made to the above two experiments, with the following addition: From t = 50s to 60s, the tires are fully slipping; $\kappa \geq 1$, all three observers fail to estimate the slip angle. When tires are slipping completely, higher order dynamics, such as carcass deformation and lateral force transfer, become significant. These unmodelled dynamics ultimately lead to failed estimation.

The figures demonstrates that the LLP method tracks the actual slip angle well in both linear and non-linear slip

regions; in certain cases, LLP outperforms both LL and LP. This is noted by comparing the average variances between the three methods, shown in Tables I and II.

TABLE I: avg. error variance of slip angle: const. speed (0s - 40s)

Estimator	Const. Steering front/rear	Slalom front/rear	Ramp Steering front/rear
LL	4.48 / 8.56	3.82 / 4.80	2.28 / 8.48
LP	0.48 / 3.70	0.48 / 2.36	0.08 / 1.94
LLP	1.94 / 7.56	1.01 / 3.67	0.16 / 0.63

TABLE II: avg. error variance of slip angle: accelerating (40s+)

Estimator	Const. Steering front/rear	Slalom front/rear	Ramp Steering front/rear
LL	3.73 / 3.86	1.50 / 1.52	22.14 / 21.50
LP	75.12 / 78.31	4.43 / 5.87	409.65 / 377.99
LLP	3.68 / 3.49	1.17 / 1.41	21.32 / 18.62

From Tables I and II, it can be observed that with no significant longitudinal acceleration present, LP tracks the actual slip angle with the smallest error; while LL tracks the slip angle with reasonable error. With pneumatic trail information incorporated, the tracking variance is reduced, as shown in the error variance of LLP. In the acceleration case, LP does not track the slip angle reasonably. LL is able to track the slip angle in a reasonable manner. LLP exhibits most accurate tracking with the lowest error variance, even in situations with longitudinal dynamic present, or when tires begin to saturate.

In terms of the slip circle presented in Section I, the above simulations demonstrated that the observer design presented in this paper, LLP, is able to achieve accurately estimation near the centre of slip circle, where low longitudinal and lateral dynamics are present. Through the slalom and the ramping test, it is shown that the observer can also estimate the slip angles well near the edge of the slip angle, where significant longitudinal dynamics are present, to the point where friction limit is reached.

V. Conclusion

The proposed observer integrates a linear observer with Dugoff tire model and a pneumatic trail estimator. This design is fast to operate, and does not require expensive sensors. It uses pneumatic trail to accurately estimate the slip angle in the tire's non-slip region. Using the Dugoff tire model, it is also able to accurately track the slip angle into the slip region of the tire, even with a significant amount of longitudinal dynamics present. As verified by the three simulated test scenarios, this observer design consistently outperforms other common observer designs.

As future improvements for this paper, stability proof of the proposed observer will be demonstrated in the sense of Lyapunov. To validate this approach, experimental data will also be gathered from an actual test vehicle and run through the estimation algorithm. Additionally, the vehicle model could be modified to a more accurate four-wheel vehicle model to account for other vehicle dynamics.

References

[1] E Bakker, H.B. Pacejka, and L. Lidner. A New Tire Model with an Application in Vehicle Dynamics Studies. In 4^{th} *Autotechnologies Conference, Monte Carlo*, 1989.

[2] D.M. Bevly, J. Ryu, and J. C. Gerdes. Integrating INS Sensors with GPS Measurements for Continuous Estimation of Vehicle Sideslip, Roll, and Tire Cornering Stiffness. *IEEE Transactions on Intelligent Transportation Systems*, 7(4):483–493, 2006.

[3] Jamil Dakhlallah, Sébastien Glaser, Said Mammar, and Yazid Sebsadji. Tire-road forces estimation using extended Kalman filter and sideslip angle evaluation. In *American Control Conference, 2008*, pages 4597–4602. IEEE, 2008.

[4] M. Doumiati, A. Victorino, A. Charara, and D. Lechner. Unscented Kalman filter for real-time vehicle lateral tire forces and sideslip angle estimation. In *Intelligent Vehicles Symposium, 2009 IEEE*, pages 901–906, 2009.

[5] Rami Y Hindiyeh and J Christian Gerdes. Equilibrium analysis of drifting vehicles for control design. ASME, 2009.

[6] Y.-H.J. Hsu, S.M. Laws, and J.C. Gerdes. Estimation of Tire Slip Angle and Friction Limits using Steering Torque. *IEEE Transactions on Control Systems Technology*, 18(4):896–907, 2010.

[7] Yung-Hsiang Judy Hsu and J. Christian Gerdes. The predictive nature of pneumatic trail: Tire Slip Angle and Peak Force Estimation using Steering Torque. In *Symposium on Advanced Vehicle Control (AVEC), Kobe, Japan*, 2008.

[8] Krisada Kritayakirana and J Christian Gerdes. Autonomous vehicle control at the limits of handling. *International Journal of Vehicle Autonomous Systems*, 10(4):271–296, 2012.

[9] Hans B Pacejka. *Tire and vehicle dynamics*. Butterworth-Heinemann, 2012.

[10] S. M. Vijaykumar R. P. Rajvardhan, S. R. Shankapal. Effect of wheel geometry parameters on vehicle steering. In *SASTech-Technical-Journal*, pages 11–18, 2010.

[11] R. Rajamani. *Vehicle Dynamics And Control*. Mechanical engineering series. Springer Science, 2006.

[12] Nicholas D Smith. Understanding parameters influencing tire modeling. *Department of Mechanical Engineering,Colorado State University*, 2004.

[13] Bin Wang, Qi Cheng, A.C. Victorino, and A. Charara. Nonlinear observers of tire forces and sideslip angle estimation applied to road safety: Simulation and experimental validation. In *International IEEE Conference on Intelligent Transportation Systems (ITSC), 2012 15th*, pages 1333–1338, 2012.

[14] Yoshiyuki Yasui, Wataru Tanaka, Yuji Muragishi, Eiichi Ono, Minekazu Momiyama, Hiroaki Katoh, Hiroaki Aizawa, and Yuzo Imoto. Estimation of lateral grip margin based on self-aligning torque for vehicle dynamics enhancement. *SAE transactions*, 113(6):632–637, 2004.